Journal of Structural Geology 48 (2013) 85–94

Contents lists available at SciVerse ScienceDirect

Journal of Structural Geology

journal homepage: www.elsevier.com/locate/jsg

Statistical tests of scaling relationships for geologic structures

Richard A. Schultz [a,*], Christian Klimczak [b], Haakon Fossen [c], Jon E. Olson [d], Ulrike Exner [e], Donald M. Reeves [f], Roger Soliva [g]

[a] ConocoPhillips Company, 600 North Dairy Ashford, Houston, TX 77079-1175, USA
[b] Department of Terrestrial Magnetism, Carnegie Institution of Washington, 5241 Broad Branch Road, N.W., Washington, D.C. 20015-1305, USA
[c] Department of Geoscience, Natural History Collections, and Centre for Integrated Petroleum Research, University of Bergen, Allégaten 41, N-5007 Bergen, Norway
[d] Department of Petroleum and Geosystems Engineering, The University of Texas at Austin, Austin, TX 78712, USA
[e] Department of Geology and Palaeontology, Natural History Museum, Burgring 7, 1010 Vienna, Austria
[f] Division of Hydrologic Sciences, Desert Research Institute, 2215 Raggio Parkway, Reno, NV 89512, USA
[g] Université Montpellier II, Laboratoire Géosciences Montpellier, Place E. Bataillon, 34095 Montpellier Cedex 5, France

ARTICLE INFO

Article history:
Received 9 March 2012
Received in revised form
10 December 2012
Accepted 11 December 2012
Available online 4 January 2013

Keywords:
Scaling
Faulting
Displacement–length scaling
Deformation bands
Compaction bands

ABSTRACT

Displacement–length data from dilatant fractures (joints, veins, igneous dikes) and several varieties of deformation bands were analyzed statistically to investigate the applicability of mechanical models proposed for their formation. All 17 datasets are generally consistent with equilibrium or long-term power-law slopes on the displacement–length diagram of either 1.0 or 0.5. Similar to many faults, disaggregation deformation bands are consistent with a power-law scaling relation having a slope of approximately $c = 1$, implying a linear dependence of maximum displacement and discontinuity length ($D_{max} = \gamma L$). In contrast, dilatant fractures, cataclastic deformation bands, and shear-enhanced compaction bands are consistent with a power-law scaling relation with a slope of approximately $c = 0.5$, implying a dependence of maximum displacement on the square root of length ($D_{max} = \alpha L^{1/2}$). The scaling relations represent an average, or long-term equilibrium outcome of deformation for conditions such as length-scale, time-scale, temperature, chemistry, and an effectively homogeneous far-field stress field, allowing for variations such as rapid and/or localized behaviors. The displacement–length scaling of these geologic structures follows systematic relationships that provide information on host-rock properties and the physics of fracture and deformation-band propagation.

1. Introduction

The basic mechanical controls on the propagation and growth of a wide range of geologic structures, including joints, faults, veins, dikes, and deformation bands, can be investigated and understood by statistical analysis of the geometric attributes of the populations of the structures. These structures develop during progressive strain localization with many key characteristics showing general scaling relationships over some particular set of conditions such as length-scale. The scaling relations are interpreted to describe an average, or long-term equilibrium value, with departures resulting from processes occurring over shorter timescales and particular spatial scales (e.g., Kim et al., 2004). Numerous studies in the literature suggest that a subset of variables exert a primary influence on the scaling; length and displacement appear to collectively capture the main aspects of loading conditions, strain accumulation during structural development, and evolving rock properties. The empirical data can then be used to test the scaling predictions of theoretical models for the growth of the geologic structures.

A fault can be described as a sharp structural discontinuity, defined in three dimensions by its slip surfaces and related structures including fault core, secondary structures, and damage zones that formed at any stage or location in the evolution of the structure. Ductile deformation structures such as drag or faulted fault-propagation folds are sometimes included in the definition along with clay smearing or other early forms of strain localization (e.g., Kim et al., 2004; Schultz and Fossen, 2008). Despite this rather comprehensive description, many studies have however demonstrated the existence of basic scaling relationships for faults, including displacement vs. length (e.g., Kim and Sanderson, 2005), fault-zone thickness vs. displacement (e.g., Childs et al., 2009; Aydin and Berryman, 2010), stepover geometry (separation vs. overlap; Aydin and Nur, 1982; Soliva and Benedicto, 2004; de Joussineau and Aydin, 2009; Long and Imber, 2011), and displacement vs. segmentation (Wesnousky, 1988; de Joussineau and Aydin,

* Corresponding author.
E-mail addresses: Richard.A.Schultz@conocophillips.com, oriongeo@gmail.com (R.A. Schultz).

0191-8141/$ – see front matter © 2012 Elsevier Ltd. All rights reserved.
http://dx.doi.org/10.1016/j.jsg.2012.12.005

2009). Comparable scaling relations have been identified for opening-mode structures, such as joints, veins, and dikes (e.g., Olson, 2003) and deformation bands (e.g., Fossen et al., 2007; Tembe et al., 2008; Ballas et al., 2012; Schultz and Soliva, 2012; Tondi et al., 2012; Soliva et al., in press).

Values for the maximum displacements D_{max} (i.e., shear offset) and horizontal lengths L of faults can be related for the long-term, equilibrium case by $D_{max} = \gamma L^c$, with c for fault populations commonly being in the approximate range of 1.0 (e.g., Cowie and Scholz, 1992a; Clark and Cox, 1996; Bailey et al., 2005; Twiss and Marrett, 2010). Fault populations can define an approximately linear dependence of maximum shear displacement and discontinuity length ($D_{max} = \gamma L$) with γ dependent on several factors, including host-rock stiffness and shear driving stress (e.g., Cowie and Scholz, 1992a; Gudmundsson, 2004; Scholz, 2002, p. 116; Schultz et al., 2006). However, these power-law scaling relations require certain conditions including effectively homogeneous far-field stress fields. Departures from these ideal conditions, such as stratigraphic or mechanical layering in which structures are initially growing, can lead to transient or local scaling relations such as non-linear displacement–length scaling, exponential length or displacement systematics, and uniform spacing. Such transient or local departures from the long-term, equilibrium power-law scaling relation are related to processes such as growth by segment linkage (Cartwright et al., 1995) and stratigraphic restriction (Soliva et al., 2005). Fault scaling relations thus represent fundamental relationships in structural geology and rock mechanics, conceptually paralleling Byerlee's rule for frictional sliding (e.g., Kohlstedt et al., 1995).

Although the scaling of dilatant structures is well recognized, its quantification and interpretation also remain somewhat controversial. Early work by Vermilye and Scholz (1995) suggested that veins (Bons et al., 2012) and igneous dikes (Rubin, 1995) scale, in the long-term or equilibrium sense, as $c = 1$, similar to faults. However, Olson (2003) proposed a theoretical model based on linear elastic fracture mechanics (LEFM) that predicted square root scaling to be dominant in opening-mode fractures. Re-analysis of a subset of the Vermilye and Scholz (1995) data as well as igneous dike data (Delaney and Pollard, 1981) showed that many veins and dikes are better described to scale approximately as $c = 0.5$ instead ($D_{max} = \alpha L^{1/2}$, where D_{max} is the maximum kinematic aperture), which is consistent with growth under conditions of constant near-tip rock properties (i.e. a critical opening-mode stress intensity factor, K_{Ic}). After publication of Olson's (2003) paper, more datasets for dilatant structures became available (see compilations by Klimczak et al., 2010 and Schultz et al., 2010). This interpretation of sub-linear scaling has been challenged by Scholz (2010, 2011), who advocated a linear scaling relation (i.e., $c = 1.0$) for dilatant fractures, similar to the scaling of faults (see Olson and Schultz, 2011 for discussion). The continuing controversy about the scaling of dilatant structures motivates a statistical assessment of their scaling properties.

Displacement–length data are also available for three varieties of deformation bands: disaggregation bands, cataclastic shear deformation bands, and shear-enhanced compaction bands. Disaggregation bands are non-cataclastic and form by shear localization in sediments and poorly consolidated sedimentary rocks with negligible volume change within the bands (e.g., Fossen, 2010; Brandes and Tanner, 2012). Cataclastic shear deformation bands are shear localization structures along which band-parallel shear displacement (typically 1–3 cm) is accompanied by a much smaller band-normal compaction that is usually a fraction of a millimeter and related to porosity reduction within the bands (e.g., Fossen et al., 2007). These bands are termed cataclastic shear bands in this paper for simplicity. Shear-enhanced compaction bands may also involve some cataclasis and grain-contact dissolution in addition to porosity reduction by grain reorganization. For these bands, the magnitude of volumetric offset is considered to be comparable to, or somewhat less than, the shear offset (e.g., Eichhubl et al., 2010; Schultz and Soliva, 2012; Soliva et al., in press).

The scaling of dilatant fractures or cataclastic shear deformation bands that both accommodate some degree of volumetric change across them was suggested to be consistent with equilibrium or long-term power-law slopes of approximately 0.5 by various workers, including Fossen and Hesthammer (1997), Rudnicki et al. (2006), Fossen et al. (2007), Rudnicki (2007), Tembe et al. (2008), Schultz et al. (2008a, 2010), and Schultz and Soliva (2012). One interpretation of this scaling relation involves propagation and growth of deformation bands at a critical value of stress intensity factor combined with appropriate remote loading conditions in a manner similar to opening-mode structures (e.g., Olson, 2003). Another interpretation invokes band thickening during propagation with only modest, non-singular stress changes at band tips (Chemenda, 2011). A definitive empirical assessment of the equilibrium scaling relation for dilatant fractures and deformation bands could inform a discussion of the primary factors controlling their propagation and growth.

In this paper, we statistically evaluate displacement–length data for three varieties of opening-mode fractures (joints, veins, igneous dikes) and three varieties of deformation bands (cataclastic shear bands, disaggregation bands, and shear-enhanced compaction bands). We use the approach employed by Clark and Cox (1996) in their study of faults and discuss the implications for the growth and scaling of these common non-fault structures.

2. Approach

Displacement–length data were compiled from several sources (Fig. 1), including 10 datasets for dilatant fractures compiled by Klimczak et al. (2010) and Schultz et al. (2010), and 7 datasets for deformation bands. The deformation band datasets include two for cataclastic shear deformation bands (Fossen and Hesthammer, 1997; Wibberley et al., 2000); three for disaggregation bands, in which no cataclasis or volumetric strain is apparent (Wibberley et al., 1999; Fossen, 2010; and Exner and Grasemann, 2010); and two for shear-enhanced compaction bands (Sternlof et al., 2005; Schultz, 2009; Schultz and Soliva, 2012) (Table 1).

The data for these types of geologic structures exhibit scatter due to several factors that are well known to contribute to scatter in datasets for fault populations (e.g. Cowie and Scholz, 1992b; Schultz, 1999; Crider and Peacock, 2004), including mechanical interaction (Renshaw and Park, 1997; Olson, 2003), three-dimensional shape (Willemse et al., 1996; Schultz and Fossen, 2002), stratigraphic restriction (Nicol et al., 1996; Soliva et al., 2005; Soliva and Schultz, 2008), and measurement technique (e.g., Clark and Cox, 1996; Xu et al., 2005). An assessment of the quality of displacement–length measurements for these data sets is given in Appendix A. In general, the datasets are of sufficiently good quality and internal consistency for statistical analysis although variability exists in the level of documentation for measurement technique and uncertainties.

As noted by many including Cowie and Roberts (2001), no geologic structure is truly isolated from its neighbors, because fractures and deformation bands form and develop as part of a population and because their presence also changes the stiffness of the surrounding rock (e.g., Kachanov, 1992; Olson, 2003). The effect of fault or joint interaction on the scaling relations was investigated quantitatively by Willemse et al. (1996), Willemse (1997), and Olson (2003). Interaction contributes to increased scatter in the scaling relations (Xu et al., 2005), with the increased or decreased

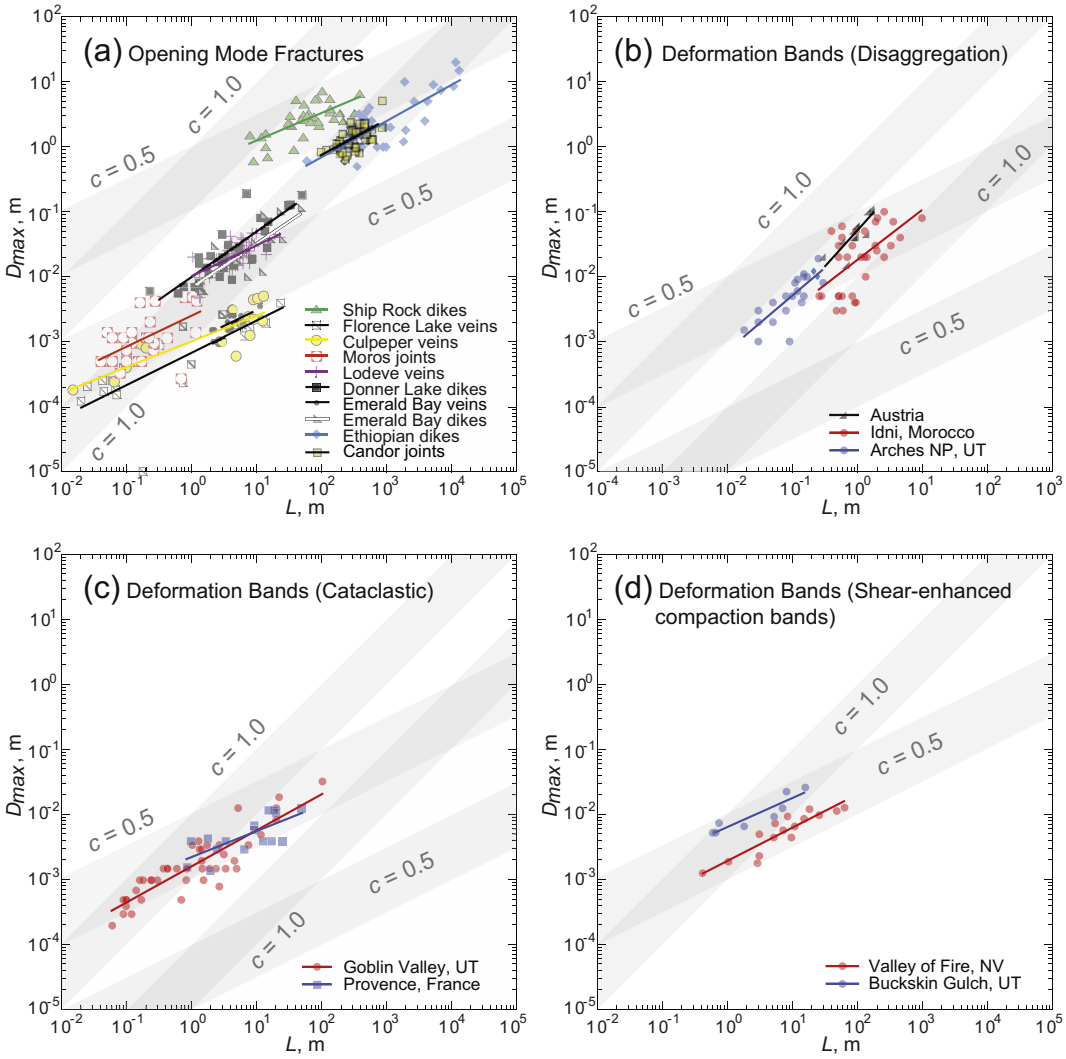

Fig. 1. Calculated best-fit slopes to displacement–length data for (a) opening-mode fractures, (b) disaggregation bands, (c) cataclastic deformation bands, and (d) shear-enhanced compaction bands. Shaded bands indicate orientations of $c = 1.0$ or $c = 0.5$ scaling on each diagram.

displacement at a given length depending on the segmentation geometry and propagation process (growth by segment linkage or radial propagation). Segmentation can also decrease the average scaling exponent, as shown by numerical simulations for mode-I fractures by Olson (2003). Reductions in scaling exponent can occur for either equilibrium case ($c = 1$ or $c = 0.5$).

Displacement–length scaling relations and a single power-law fit are recognized to be applicable to individual datasets only, rather than to a compiled dataset containing structures in different rock types, depths, and locations (Cowie and Scholz, 1992a; Clark and Cox, 1996; Twiss and Marrett, 2010). This condition is due, in part, because variations in modulus, yield strength, or critical opening-mode stress intensity factor of the host rock contribute to vertical shifts in position of the data on the displacement–length diagram (e.g. Cowie and Scholz, 1992a; Schultz and Fossen, 2002; Olson, 2003; Gudmundsson, 2004), leading to poorer fits and different slopes than would be appropriate to the individual datasets themselves. Consequently, we analyze the statistics of each dataset listed in Table 1 separately.

Standard regression techniques and hypothesis testing (i.e., *t*-statistic) were employed in our study to determine the relationship between fracture (generically-defined here) displacement and length. Other approaches, such as maximum likelihood estimation techniques while effective (Clauset et al., 2009), are specifically formulated to estimate distributional properties for a single random variable, such as length or displacement. Given that our investigation focuses on the relationship or correlation between two variables: length and displacement, standard regression methods are required.

We analyzed 19 datasets, including our 17 non-fault data sets and two for faults (Clark and Cox, 1996) to verify the coherence in methods. We used the statistical computing package MINITAB (Release 15, Minitab statistical software, www.minitab.com) for the regression analysis.

The correlation of maximum displacements (D_{max}) to lengths (L) has the general form

$$D_{\max} = \frac{1}{P}L^{c}, \tag{1}$$

where P and c are dataset-specific constants. Eq. (1) can be rewritten as

$$\begin{aligned} \log D_{\max} &= K + c\log L, \\ K &= -\log P \end{aligned} \tag{2}$$

Table 1
Statistical evaluation of datasets for fractures and deformation bands. n = number of fractures or deformation bands in a given dataset, $\hat{C}_i$ = estimate of power-law exponent c, SE(C) = standard error of the estimate, $t_{1.0}$ = standard t-statistic for hypothesis that $c = 1.0$, $t_{0.5}$ = t-statistic for hypothesis that $c = 0.5$, σ_i = residual standard deviation around best-fit line, R = goodness-of-fit correlation coefficient, R^{2i} = coefficient of determination of the best-fit regression line, $R^2_{1.0}$ = coefficient of determination of best-fit line having $c = 1.0$, $R^2_{0.5}$ = coefficient of determination of best-fit line having $c = 0.5$.

Fracture type	i	Datasets	n	$\hat{C}_i$	SE ($\hat{C}_i$)	$t_{1.0}$	$t_{0.5}$	σ_i	R	R^{2i}	$R^2_{1.0}$	$R^2_{0.5}$
Faults												
	1	Elliott (1976) Thrust Faults	29	1.0143	0.0845	0.1692	6.0863	0.1763	0.9177	0.8421	0.8420	0.6256
	2	Krantz (1988) Normal Faults	16	1.4439	0.2270	1.9555	4.1581	0.2776	0.8619	0.7429	0.6727	0.4254
Opening mode fractures												
	3	Schultz et al. (2010) Candor Joints	32	0.5324	0.1194	−3.9162	0.2714	0.1523	0.6312	0.3985	0.0910	0.3970
	4	Delaney and Pollard (1981) Shiprock	35	0.4325	0.0763	−7.4380	−0.8849	0.1890	0.7024	0.4933	Uncorrelated	0.4813
	5	Vermilye and Scholz (1995) Florence Lake Veins	22	0.4916	0.0815	−6.2425	−0.1037	0.3925	0.8035	0.6455	Uncorrelated	0.6453
	6	Vermilye and Scholz (1995) Culpeper Veins	16	0.3941	0.0626	−9.6797	−1.6925	0.2356	0.8596	0.7389	Uncorrelated	0.6855
	7	Moros (1999) Joints	28	0.4789	0.1357	−3.8401	−0.1555	0.3209	0.5691	0.3239	Uncorrelated	0.3233
	8	Schultz et al. (2008a) Lodève Veins	46	0.4703	0.0814	−6.5072	−0.3654	0.1518	0.6567	0.4313	Uncorrelated	0.4295
	9	Schultz et al. (2008b) Ethiopian Dikes	34	0.5542	0.0760	−5.8676	0.7131	0.2523	0.7902	0.6244	0.2203	0.6185
	10	Klimczak et al. (2010) Donner Lake Dikes	28	0.6915	0.0850	−3.6299	2.2538	0.2452	0.8474	0.7181	0.5752	0.6630
	11	Klimczak et al. (2010) Emerald Bay Veins	14	0.5521	0.1154	−3.8813	0.4515	0.0838	0.8100	0.6561	0.2244	0.6502
	12	Klimczak et al. (2010) Emerald Bay Dikes	14	0.6758	0.1600	−2.0263	1.0988	0.2763	0.7731	0.5977	0.4602	0.5573
Deformation bands (Cataclastic)												
	13	Fossen and Hesthammer (1997) Goblin Valley	44	0.5547	0.0461	−9.6624	1.1859	0.2332	0.8804	0.7752	0.2755	0.7677
	14	Wibberley et al. (2000) Provence	16	0.3988	0.1007	−5.9702	−1.0050	0.2093	0.7269	0.5284	Uncorrelated	0.4943
Disaggregation bands												
	15	Exner and Grasemann (2010) Austria	12	1.0240	0.2217	0.1083	2.3636	0.1582	0.8252	0.6809	0.6805	0.5026
	16	Wibberley et al. (1999) Idni	33	0.7626	0.1940	−1.2237	1.3536	0.3991	0.5767	0.3326	0.3003	0.2931
	17	Fossen et al. (2007) Arches	21	0.8427	0.1515	−1.0384	2.2619	0.2240	0.7813	0.6104	0.5891	0.5094
Shear-enhanced compaction bands												
	18	Sternlof et al. (2005) Valley of Fire	16	0.5100	0.0645	−7.5947	0.1548	0.1433	0.9038	0.8169	0.0628	0.8166
	19	Schultz (2009) Buckskin Gulch	8	0.4398	0.0798	−7.0237	−0.7549	0.1194	0.9139	0.8352	Uncorrelated	0.8195

Eqs. (1) and (2) do not account for data scatter, but Eq. (2) can be modified to account for scatter (Clark and Cox, 1996):

$$\log D_{ij} = K_i + c_i \log L_{ij} + \Delta_{ij}, \quad (3)$$

where (D_{ij}, L_{ij}) represents the j-th pair of the measurements in the i-th dataset, K_i and c_i represent the intercept and slope of the best-fit D–L function in log–log space, and Δ_{ij} are the random errors in measurement. The 19 best-fit regression lines, as described by Eq. (3), were statistically generated (Table 1). As in Clark and Cox (1996), the probability of the 19 estimated slopes being equivalent to either of the hypothesized slopes of $c = 1.0$ and $c = 0.5$ was tested by using the t-statistic. Resulting t-values of −2 to 2 then confirm the given hypothesis at a confidence interval of 95%. The t-statistic counts the number of standard errors that the estimate is from the hypothesis, which can yield better t-values for datasets with greater standard errors. Because it accounts for the relatively small number of observations within each dataset, the scatter around the fitted line, and the possibly unequal spacing of the log L values within the dataset (Clark and Cox, 1996), the t-statistic is a good statistical measure for evaluation of our datasets.

3. Statistical results

Results show that displacement–length (D/L) relationships can have slopes ranging from as low as $c_i = 0.2$ to up to $c_i = 1.6$ (Table 1). Judging by the t-statistic, the hypothesized slope of $c = 1.0$ can be statistically ruled out for all of the opening mode datasets (entries under $t_{1.0}$ in Table 1 with absolute values > 2). On the other hand, hypothesized slopes of $c = 0.5$ are statistically admissible for all of the opening-mode datasets except for the Donner Lake dikes (entries under $t_{0.5}$ in Table 1). For both cataclastic shear bands and shear-enhanced compaction bands, t-values support the hypothesis of $c = 0.5$ and at the same time rule out slopes of $c = 1.0$ (entries under $\hat{C}_i$ in Table 1). Similar to faults, the t-statistic for disaggregation bands indicates that a hypothesized slope of $c = 1.0$ are admissible for this dataset (Table 1). Some datasets, e.g. Ship Rock dikes, Moros joints (Fig. 1a), and the Idni disaggregation bands (Fig. 1b), show scatters that visually appear to suggest steeper slopes than the best-fit regression curve. However, as the best-fit line is a statistically derived curve centered to the cluster of data points, it represents the line of least error with respect to the overall scatter of the data and thus, quantitatively is the appropriate relationship between length and displacement. The Emerald Bay dike dataset exhibits a slope between 0.5 and 1.0, however, this result likely reflects difficulty in measuring displacements and lengths for isolated dike segments given the rugged three-dimensional exposure plus the wide range of dike linkage and related geometries (Klimczak et al., 2010).

The goodness-of-fit statistic measures how well a model prediction explains a given set of data (e.g. Navidi, 2006). For linear relationships, such as given by Eq. (3) for the D/L data, the goodness-of-fit statistic can be expressed by the coefficient of correlation, R, which is a measure of the clustering of the data

around the best-fit regression line. The strength of the best-fit regression line can also be expressed by the square of the correlation coefficient, the coefficient of determination, R^2, which relates the overall spread of data points around the center of the cluster to the overall spread of data points around the best-fit regression line. Values for the coefficient of determination can range between $R^2 = 0$ for uncorrelated data and $R^2 = 1$ for perfect correlation.

To investigate how strongly the D/L datasets correlate, we determined the coefficients of correlation and determination. In addition, we computed the fitted coefficient of determination for the hypothesized slopes of $c = 1.0$ and $c = 0.5$ to test the strength of correlation of the proposed D/L relationships against the data. The details of this analysis are given in Appendix B. Results of the goodness-of-fit statistic show that in all datasets, displacements strongly correlate with lengths. Correlation coefficients range between $R = 0.57$ to $R = 0.92$, averaging $R = 0.78$.

The fitted coefficient of determination statistic confirms the trends of the t-statistic. Opening and closing-mode structures display stronger correlations for slopes of $c = 0.5$. The fitted R^2-values ($R^2_{0.5}$) are very close to R^2-values of the best-fit line (R^{2i}). Coefficients of determination for fitted slopes of $c = 1.0$ for the opening and closing-mode structures are either very poor or entirely uncorrelated (Table 1). Disaggregation bands show a stronger correlation with a slope of $c = 1.0$ than with a slope of $c = 0.5$.

4. Discussion and implications

The statistical analysis of our displacement–length data for opening-mode fractures and several types of deformation bands permits determination of their scaling exponents. The opening-mode fractures, including joints, veins, and igneous dikes, are statistically consistent with a scaling exponent of $c = 0.5$, which is in agreement with recent previous investigations (Olson, 2003; Schultz et al., 2008a; Klimczak et al., 2010). In contrast to faults, opening-mode fractures thus follow a scaling law of the form $D_{max} = \alpha\sqrt{L}$, implying that their propagation might depend on locally constant values of modulus and critical opening-mode stress intensity factor that are specific to the host-rock or scale of fracturing at the time of deformation (Olson, 2003). These likely vary from location to location, between events widely separated in time, or between events driven at significantly different temperatures (e.g., veins filled by aqueous solutions vs. dikes filled by magma). Several investigators have identified specific influencing factors such as in-situ stress magnitude, rock tensile strength, chemical kinetics, scale of the rock mass, and temperature (e.g., Pollard, 1987; Rubin, 1993; Bunger, 2008; Schultz et al., 2008b; Olson and Schultz, 2011).

Fracture segmentation decreases the power-law exponent for a given sample of fractures or deformation bands from its long-term or equilibrium value, regardless of whether that equilibrium value is 1.0 (the particular case illustrated by Olson, 2003) or 0.5. Rather than invalidating a scaling model that is based on the physics of fracture-related processes, mechanically interacting (soft-linked or echelon) fractures such as veins and dikes demonstrate a clear scaling relationship in which the departures from an equilibrium value can be traced to local permutations in displacement within an array.

Echelon arrays of segmented veins and dikes are sometimes interpreted as resulting from mixed-mode I–III propagation of a parent structure. Theoretical breakdown criteria for this case consider the local stress state and initial perturbation dimension along a parent fracture (e.g., Leblond et al., 2011), but neglect material heterogeneity or mechanical interaction among segments and the parent fracture (Pollard et al., 2004). The scaling relations for veins and dikes (Fig. 1) indicate that the segments propagated, interacted, and linked (e.g., Delaney and Pollard, 1981; Fink, 1985; Nicholson and Pollard, 1985; Pollard, 1987; Rubin, 1995; Okubo and Martel, 1998; Weinberger et al., 2000) in a manner consistent with other segmented fractures or deformation bands, despite the nature of their connectivity to a parent structure.

The constitutive relation of the host rock ahead of opening-mode fractures is relevant to their scaling. In the simplest cases, both LEFM and the Dugdale models (e.g., Rubin, 1993) would predict linear displacement–length scaling if the fractures propagated at constant driving stress (because fracture toughness would need to increase with the square root of fracture length). If instead, it is assumed that fracture toughness is a constant during propagation, both the LEFM and the Dugdale model predict sublinear (i.e., $c = 0.5$) scaling of aperture with length, and a constant process zone size. The important factors for scaling in this case are whether fracture toughness and process zone size are constants. Propagation of hydraulic fractures and igneous dikes has also been studied by the use of damage mechanics (Mazars and Pijaudier-Cabot, 1996; Weinberger et al., 2000) and through the use of more complete constitutive relations for the host rock (Busetti et al., 2012) that relax the rather restrictive assumptions of the LEFM and Dugdale models (e.g., Pollard, 1987). This work shows that near-tip damage of the host rock is considerably more complicated than the LEFM and Dugdale models would suggest, with inelastic energy dissipation, shearing, shape, and dimensions of the process zone not adequately accounted for in the simpler predictions (Busetti et al., 2012). Further work is required to more thoroughly understand how near-tip energy dissipation and related factors are related to fracture scaling.

As a class of structures, deformation bands can scale approximately with either length L or $\sqrt{L}$. As hypothesized by Schultz et al. (2008a), the statistical analysis confirms that disaggregation bands scale with L. These structures accommodate primarily shear offsets with only a minor amount of volumetric change across them. In contrast, the analyzed cataclastic shear deformation bands, as well as the shear-enhanced compaction bands, scale as $\sqrt{L}$, consistent with the literature (e.g., Fossen and Hesthammer, 1997; Rudnicki et al., 2006; Rudnicki, 2007; Tembe et al., 2008; Schultz, 2009). The analysis supports the inference that grain breakage exerts an important local control on the scaling exponent for structural discontinuities. For example, recent work on compaction in chalk demonstrates that the vertical effective stress magnitude for pore collapse is related to the square root of pore size (Japsen et al., 2011). Laboratory investigations show that stiffness and strength within deformation bands change with progressive shearing, grain-size reduction, and grain reorganization (Kaproth et al., 2010; Ikari et al., 2011). These results imply that scaling of deformation bands may vary with grain fragmentation and shear strain accumulation.

The thicknesses and compactional displacements of pure (i.e., wiggly or crooked) compaction bands appear to be relatively constant for different lengths (e.g. Fossen et al., 2011), implying that these structures do not follow displacement–length scaling relations as they grow. In contrast, the thicknesses (T_{band}) of shear-enhanced compaction bands in porous sandstones scale with band length (Rudnicki, 2007; Schultz et al., 2008a; Tembe et al., 2008; Schultz, 2009), $T_{band} = \beta L^{1/2}$. The two sets of measurements of shear-enhanced compaction bands indicate that $\beta = 0.0019\ m^{1/2}$ (Valley of Fire site) and $\beta = 0.0063\ m^{1/2}$ (Buckskin Gulch site). By using a J-integral approach, following Rudnicki and Sternlof (2005) and Rudnicki (2007), Schultz and Soliva (2012) found for shear-enhanced compaction bands that $D_{max} \sim \beta\varepsilon_p L^{1/2}$, where ε_p is the normal (compactional) plastic strain that is related

both to the porosity change across the band and band thickness (Soliva et al., in press). Normal and shear strains are related trigonometrically to band thickness for shear-enhanced compaction bands, and plastic shear strain is related to the plastic normal strain through the band orientation (Schultz and Soliva, 2012). Given calculated values of $\varepsilon_p = 0.66$ or 0.0256 (Schultz and Soliva, 2012), $D_{max} = 1.25 \times 10^{-4} L^{1/2}$ and $D_s = 1.61 \times 10^{-4} L^{1/2}$ for the shear-enhanced compaction bands at Valley of Fire and Buckskin Gulch, respectively. The displacement–length scaling relations for these bands are interpreted to involve band thickening during growth for constant plastic normal strain. This interpretation is consistent with the findings of Chemenda (2011) for band localization and growth during discontinuous bifurcation of material properties in the host rock and, perhaps, with a critical stress intensity factor of individual host-rock grains (e.g., Japsen et al., 2011; Wong and Baud, 2012), rather than the host rock, for bands that exhibit grain breakage.

Several deformation mechanisms can produce shear displacements with subordinate volumetric change and grain fragmentation with $c = 1.0$ scaling. Frictional sliding and attendant faulting generally occur with shearing offsets that greatly exceed dilation along a fault, even for cases involving sliding along rough or poorly connected surfaces under conditions of low confining pressure or for critically stressed faults (e.g., Barton et al., 1995; Zoback, 2007, pp. 340–349; Zhao and Cai, 2010). The equilibrium or long-term scaling of faults (e.g., Clark and Cox, 1996) is consistent with this expectation. Shearing in unconsolidated porous granular solids by grain rolling, forming disaggregation bands (Fossen, 2010), implies that grain-flow mechanisms, that do not involve significant cataclasis, are associated with structures that scale linearly. Rotation of phyllosilicate minerals into a zone of shearing (phyllosilicate bands and clay smears; Fossen et al., 2007), as can occur in hydroplastic faults within soft siliciclastic sediments (e.g., Petit and Laville, 1987), and rotation of elongate cobbles into a preferred orientation (forming coarse-grained disaggregation bands), can also produce structures that scale as $c = 1.0$ (Exner and Grasemann, 2010). The absence of structures that result from cataclasis in these bands is consistent with their linear displacement–length scaling.

Although the scaling of fully developed faults is not the focus of this paper, the analysis suggests that fault scaling relations may be influenced by the types of earlier structures that coalesced to form the eventual fault. For example, Crider and Peacock (2004) noted that scatter in the displacement–length scaling relations may be attributed to incomplete linkage of cracks and other structures, particularly at smaller length-scales. Similarly, Nicol et al. (2010) suggested that the maturity of a fault might contribute to a scaling exponent <1.0. In both cases, if the fault formed by linkage of preexisting dilatant cracks, scatter at small length-scales could be attributed to a change in displacement–length scaling, from $\sqrt{L}$ to L, as shear displacements became predominant along the longer segments. A comparable explanation for the Chimney Rock faults (Krantz, 1988, 1989), as they developed from deformation band damage zones, was made by Fossen and Hesthammer (1997). Faulting of carbonate and low-porosity crystalline rocks that involves extensive deformation banding or jointing prior to fault slip (e.g., Tondi et al., 2006; Hatton et al., 1994) would be associated with an increase in scaling exponents during fault development. This behavior was recently demonstrated by Tondi et al. (2012) for carbonate rocks and for faulting in porous sandstone by Rotevatn and Fossen (2012). Similarly, propagation of a fault into a layer containing joints or deformation bands (e.g., Jamison, 1989; Okubo and Schultz, 2005), or nucleation of a fault on these structures (e.g., Welch et al., 2009), would likely incorporate the spatial characteristics of the fracture or band network into the initial scaling characteristics of the through-going fault. Growth of fractures and deformation bands in a heterogeneous stratigraphic sequence implies that the scaling relations would depend on the mechanical stratigraphy (Schultz and Fossen, 2002; Soliva et al., 2005; Soliva and Schultz, 2008) and, in turn, on spatially, temporally, and lithologically varying values of critical stress intensity factor for pre-existing joint sets that grew under conditions comparable to LEFM.

5. Conclusions

Statistical analysis confirms that one type of deformation band (disaggregation bands) scales approximately as $c = 1.0$, whereas other structures including dilatant (opening mode) fractures (joints, veins, and igneous dikes), cataclastic shear bands, and shear-enhanced compaction bands are best described to scale approximately as $\sqrt{L}$, or $c = 0.5$. These scaling exponents are interpreted as representing the predictions of certain theoretical growth models for conditions such as length-scale, time-scale, temperature and chemical effects, and effective homogeneity of far-field stress fields such that an average or equilibrium value of power-law scaling exponent is achieved for a given population of fractures or deformation bands. Models for the fracture or deformation band behavior such as growth by segment linkage or scaling changes due to stratigraphic restriction can predict trajectories through scattered data from a particular population that can be tested by using appropriate observations and measurements. One such trajectory, that of a long-term or equilibrium value having a power-law exponent of 1.0 or 0.5, was tested against data in this paper.

The results confirm prior interpretations that structures with predominantly shearing offsets and relatively negligible volumetric changes (i.e., dilational or compactional normal strains) or cataclasis, scale approximately linearly in displacement–length (i.e., $c = 1.0$), whereas structures with volumetric changes accommodated by grain breakage scale approximately as $\sqrt{L}$, or $c = 0.5$. The wide range of values for critical stress intensity factor implied by dilatant fracture datasets supports prior suggestions of non-universal fracture scaling (Hatton et al., 1994). Its converse would implausibly require a single value of critical stress intensity factor for any rock type or environmental condition (e.g., Scholz, 2010; cf. Olson and Schultz, 2011). More comprehensive models of fracture and deformation-band propagation through host rock that include more realistic and evolving constitutive relations, especially at the grain scale, along with integrated studies of the progressive growth and scaling of these structures would better inform our understanding of the physical controls of fracture and deformation band scaling.

Acknowledgments

We thank Jean-Pierre Petit for discussing the context of the Idni disaggregation deformation bands in Morocco, Alexandre Chemenda for his insights on propagation of deformation bands, Seth Busetti for discussions of near-tip damage near hydraulic fractures, Andy Nicol for discussing his work and insights on deformation band growth and kinematics, and Malcolm Clark and Jim Carr for discussions on the statistical treatment. Reviews by Paul Gillespie, Conrad Childs, and Editor Bill Dunne improved the manuscript. This work was supported by grants from NASA's Planetary Geology and Geophysics Program to RAS while the first author was at the University of Nevada, the Fracture Research and Application Consortium (FRAC) of The University of Texas at Austin to JEO, and the Austrian Science Fund project V151–N22 to UE. ConocoPhillips is thanked for permission to publish this work.

Appendix A

The quality of displacement–length data for the data sets investigated in this paper is briefly described in this appendix. In particular we summarize the data on the basis of outcrop quality, measurement method, and discrimination between isolated, interacting or linked structures by the original authors. We generally chose not to repeat the description of the field areas, outcrops, or structures that are contained in the original or cited sources, but instead focus on a uniform assessment of data quality from the available datasets.

All the datasets presented in Fig. 1 except for those from Moros' thesis were published in peer-reviewed papers, and are inspected in the following way. For each dataset, we consider:

a. How many datasets reported from these papers are shown on photographs?
b. How many datasets in which the measurement method has been explained?
c. How many datasets where the displacement along the fracture or deformation band was directly measured, rather than extrapolated?
d. How many datasets distinguished the geometry of the structures (e.g., isolated vs. segmented)?
e. How many datasets in which the minerals within opening-mode fractures, exclusive of igneous dikes, show synkinematic infill?

Joints

Moros, M.S. thesis (1999), 1 set (Moros joints, Fig. 1a). The thesis is not very well illustrated but the outcrop photographs show clear examples of the joints. Only isolated joints were chosen for the present analysis. The selection of which joints were measured is given in an appendix to Schultz et al. (2008a). The method of measurements is well described and the quality and resolution of displacement profile also suggest that the outcrops have preserved the joint apertures. Measurements of opening-mode displacement corresponds to the initial aperture reduced to some degree by diagenetic cement. Opening displacements measured may also be wider than initial ones due to relaxation in the near-surface stress state.

Schultz et al. (2010), 1 set (Candor joints, Fig. 1a). Sub-meter resolution of fracture lengths and displacements on Mars were obtained from the High-Resolution Imaging Science Experiment (HiRISE) camera (McEwen et al., 2007) onboard the Mars Reconnaissance Orbiter spacecraft, which acquired images at up to 25–30 cm/pixel. A well-exposed outcropping of sub-km-scale joints was documented in southwest Candor Chasma, within an exposure of layered sedimentary deposits (Okubo, 2010). Digital Elevation Models derived from stereo HiRISE images, having a vertical resolution of ~1 m/pixel, indicate that these joints are sub-vertical, dipping at 82 ± 2°. The highest resolution HiRISE observation of this area (image PSP_001984_1735) has a ground-sampling dimension of 0.26 m per pixel, so that features ~1 m in diameter can be resolved.

32 joints exhibit displacements that were measured in accordance with the estimated uncertainty and also do not appear to be connected to an adjacent fracture. Measurements between multiple tie-points along each fracture are used to establish the distribution of displacement, for apertures greater than 2 pixels (0.52 m). Inspection of the HiRISE imagery reveals a predominantly opening-mode sense of displacement between tie points on either side of the joints, with the displacement vector being approximately normal to the plane of the fracture. The resulting displacement profiles show that the maximum measured opening displacement occurs approximately at the center of the joint, indicating that mechanical interactions with adjacent fractures are minimal. Measured Martian joint lengths are between 98.0 and 859.2 m, and maximum opening displacements are 0.63–5.0 m. The dataset is of high quality and the measurements and uncertainties are well described.

Veins

Vermilye and Scholz (1995), 7 sets with 2 reexamined by Olson (2003) (Florence Lake veins, Culpeper veins, Fig. 1a). The dataset appears to be robust since only isolated veins were measured on surface exposures. Because the relative timing between the jointing and infilling by vein fluids was not addressed, for example by examining contact relations between vein walls and the sealing minerals, any potential changes in aperture leading to the present-day values are difficult to assess.

Petit et al. (1994), 1 set (Lodève veins, Fig. 1a). The measurement technique is well described, and only isolated veins were used. The measurements were verified independently in the same field locality by Soliva. Vein apertures are probably minima due to uncertain degrees of diagenetic sealing and/or relaxation of joints prior to infill.

Klimczak et al. (2010), 1 set (Emerald Bay veins, Fig. 1a) The method and uncertainties are the same as those described in the same paper for Donner Lake and Emerald Bay dikes.

Dikes

Delaney and Pollard (1981), 1 set (Ship Rock dikes, Fig. 1a). Geomechanical aspects of dike injection are better developed than geological observation, but the geology and measurement method are better documented than many other similar studies. Here it is clear that the measured opening-mode displacements correspond to the real kinematic apertures, since the magmatic fluid pressure allows the fractures to grow. Some erosion or tubing of magma can affect the measurements (as shown on displacement profiles) and the dikes are commonly interacting as part of echelon arrays. Most segments are not isolated, which probably contributes to the large scatter observed in the data set.

Klimczak et al. (2010), 2 sets (Donner Lake dikes, Emerald Bay dikes, Fig. 1a). The method and uncertainties are described and since the fractures are dikes, measured displacements correspond to the real kinematic aperture. The potential effect of segmentation on the scaling relations was not explicitly addressed. Rugged three-dimensional exposures of Donner Lake dikes, with topographic heterogeneity on the same scale as dike segmentation, hindered the identification and measurement of isolated dike segments.

Schultz et al. (2008b), 1 set (Ethiopian dikes, Fig. 1a). The method and uncertainties are described. Here it is also clear that the real kinematic aperture has been measured since they are dikes. The method has been described (image analysis). Dike segmentation was investigated and the individual dike segments were used.

Deformation bands

Fossen and Hesthammer (1997), 1 set (Goblin Valley, UT, Fig. 1c). Isolated bands are separated from segmented bands and give the same trend as the segmented ones but with less scatter. Bands and measurements are well described. Some uncertainty occurs due to the choice of stratigraphic lamination for correlation can occur since the cross-cut markers are not always well defined.

Wibberley et al. (1999), 1 set (Idni, Morocco, Fig. 1b). The dataset appears robust since only isolated bands were measured on bedding planes having offset markers. However, no field photographs were provided and there is no discussion of the potential effect of erosion on the measurements.

Wibberley et al. (2000), 1 set (Provence, France, Fig. 1c). This dataset contains clear measurements of displacement obtained from the cross-cutting of one band by another. Good precision of measurement was achieved. The method is well described but some uncertainty comes from the fact that the offset marker is a band and not a simple passive marker. The offsets are therefore underestimates since the cutting band could exist before the cut band. Band displacements and lengths were measured in cross-section, whereas the other datasets were measured in map view. The general consistency between the deformation band datasets suggests that the viewing geometry of bands contributes only a relatively small amount, if at all, to differences in the scaling relations as a function of orientation.

Sternlof et al. (2005), 1 set (Valley of Fire, NV, Fig. 1d). Measurements of band thicknesses are generally well described and an estimation of compaction within the bands based on measured porosity reduction was provided.

Schultz (2009), 1 set (Buckskin Gulch, UT, Fig. 1d). Measurement technique and uncertainties are well described; only isolated bands were measured. Band thicknesses, rather than compactional displacements, were measured following Sternlof et al. (2005), making conversion of thickness to offset a source of uncertainty (but see discussion by Schultz and Soliva, 2012).

Exner and Grasemann (2010), 1 set (Austria, Fig. 1b). A clear description of both the disaggregation bands and the method to measure the offset is provided. The quality of the measurements is very good since the stratigraphy is very well expressed providing unambiguous passive markers.

Fossen (2010), 1 set (Arches National Park, UT, Fig. 1b). The geologic and stratigraphic setting of the bands is well described, as are their main characteristics. The Arches disaggregation bands are almost completely invisible except where lamination is present and offset in the sandstone, and they appear to primarily accommodate shearing strains. They are overprinted by the cataclastic deformation bands described by Antonellini et al. (1994). The measurements were obtained on surfaces where laminae more resistant to weathering exhibit the displacement variations along the bands.

Appendix B

The coefficient of determination is the ratio of the regression sum of squares, the difference of total sum of squares and error sum of squares, to the total sum of squares, given as:

$$R^2 = \frac{\sum_{j=1}^{n}\left(y_{ij}-\overline{y}_i\right)^2-\sum_{j=1}^{n}\left(y_{ij}-\widehat{y}_{ij}\right)^2}{\sum_{j=1}^{n}\left(y_{ij}-\overline{y}_i\right)^2}, \tag{B1}$$

where $y_{ij}-\overline{y}_i$ represent the difference of the j-th y-value of the i-th dataset to the average y-value of i-th dataset, $\overline{y}_i$, and $y_{ij}-\widehat{y}_{ij}$ represents the prediction error as the difference of the j-th y-value of the i-th dataset to the regression line. The predicted y-value, $\widehat{y}_{ij}$, is expressed as

$$\widehat{y}_{ij} = \overline{y}_i + c_i\left(x_{ij}-\overline{x}_i\right), \tag{B2}$$

with c_i being the slope of the best-fit regression line of the i-th dataset, and $(x_{ij}-\overline{x}_i)$ representing the difference of the j-th x-value of the i-th dataset to the average x-value of i-th dataset. As apparent from Eq. (B2), the best-fit regression line is centered at the cluster of data points, running through the average x- and y-values, $\overline{x}_i$ and $\overline{y}_i$.

For our fitted coefficient of determination statistic, we substituted the best-fit slope c_i (Table 1) with the hypothesized slopes of $c = 1.0$ and $c = 0.5$ to investigate whether correlation exists of data at these slopes as well as which slope yield stronger correlations. As for the best-fit regression line, the regression lines with the hypothesized slopes are also centered at the cluster of data points, therefore yielding comparable results. Since the coefficient of determination is at its maximum for the best-fit line, fitted R^2-values are lower.

References

Antonellini, M., Aydin, A., Pollard, D.D., 1994. Microstructure of deformation bands in porous sandstones at Arches National Park, Utah. Journal of Structural Geology 16, 941–959.

Aydin, A., Berryman, J.G., 2010. Analysis of the growth of strike-slip faults using effective medium theory. Journal of Structural Geology 32, 1629–1642.

Aydin, A., Nur, A., 1982. Evolution of pull-apart basins and their scale independence. Tectonics 1, 11–21.

Bailey, W.R., Walsh, J.J., Manzocchi, T., 2005. Fault populations, strain distribution and basement fault reactivation in the East Pennines Coalfield, UK. Journal of Structural Geology 27, 913–928.

Ballas, G., Soliva, R., Sizun, J.-P., Benedicto, A., Cavilhes, T., Raynaud, S., 2012. The importance of the degree of cataclasis in shear bands for fluid flow in porous sandstone (Provence, France). American Association of Petroleum Geologists Bulletin 96, 2167–2186.

Barton, C.A., Zoback, M.D., Moos, D., 1995. Fluid flow along potentially active faults in crystalline rock. Geology 23, 683–686.

Bons, P.D., Elburg, M.A., Gomez-Rivas, E., 2012. A review of the formation of tectonic veins and their microstructures. Journal of Structural Geology 43, 33–62.

Brandes, C., Tanner, D.C., 2012. Three-dimensional geometry and fabric of shear deformation-bands in unconsolidated Pleistocene sediments. Tectonophysics 518–521, 84–92.

Bunger, A.P., 2008. A rigorous tool for evaluating the importance of viscous dissipation in sill formation: it's in the tip. In: Annen, C., Zellmer, G.F. (Eds.), Dynamics of Crustal Magma Transfer, Storage and Differentiation. Geological Society, London, Special Publication, vol. 304, pp. 71–81.

Busetti, S., Mish, K., Hennings, P., Reches, Z., 2012. Damage and plastic deformation of reservoir rocks: part 2. Propagation of a hydraulic fracture. American Association of Petroleum Geologists Bulletin 96, 1711–1732.

Cartwright, J.A., Trudgill, B.D., Mansfield, C.S., 1995. Fault growth by segment linkage: an explanation for scatter in maximum displacement and trace length data from the Canyonlands Grabens of SE Utah. Journal of Structural Geology 17, 1319–1326.

Chemenda, A.I., 2011. Origin of compaction bands: anti-cracking or constitutive instability? Tectonophysics 499, 156–164.

Childs, C., Manzocchi, T., Walsh, J.J., Bonson, C.G., Nicol, A., Schöpfer, M.P.J., 2009. A geometric model of fault zone and fault rock thickness variations. Journal of Structural Geology 31, 117–127.

Clark, R.M., Cox, S.J.D., 1996. A modern regression approach to determining fault displacement-length relationships. Journal of Structural Geology 18, 147–152.

Clauset, A., Shalizi, C.R., Newman, M.E.J., 2009. Power-law distributions in empirical data. Society for Industrial and Applied Mathematics Review 51, 661–703. http://dx.doi.org/10.1137/0707/10111. arXiv:0706.1062v2 [physics.data-an].

Cowie, P.A., Roberts, G.P., 2001. Constraining slip rates and spacings for active normal faults. Journal of Structural Geology 23, 1901–1915.

Cowie, P.A., Scholz, C.H., 1992a. Physical explanation for the displacement-length relationship of faults using a post-yield fracture mechanics model. Journal of Structural Geology 14, 1133–1148.

Cowie, P.A., Scholz, C.H., 1992b. Displacement-length scaling relationships for faults: data synthesis and discussion. Journal of Structural Geology 14, 1149–1156.

Crider, J.A., Peacock, D.C.P., 2004. Initiation of brittle faults in the upper crust: a review of field observations. Journal of Structural Geology 26, 691–707.

de Joussineau, G., Aydin, A., 2009. Segmentation along strike-slip faults revisited. Pure and Applied Geophysics 166, 1575–1594.

Delaney, P.T., Pollard, D.D., 1981. Deformation of Host Rocks and Flow of Magma during Growth of Minette Dikes and Breccia-bearing Intrusions Near Ship Rock, New Mexico. U.S. Geological Survey, Professional Paper 1202, 61 pp.

Eichhubl, P., Hooker, J.N., Laubach, S.E., 2010. Pure and shear-enhanced compaction bands in Aztec Sandstone. Journal of Structural Geology 32, 1873–1886.

Elliott, D., 1976. The energy balance and deformation mechanisms of thrust sheets. Philosophical Transactions of the Royal Society, London A283, 289–312.

Exner, U., Grasemann, B., 2010. Deformation bands in gravels: displacement gradients and heterogeneous strain. Journal of the Geological Society, London 167, 905–913.

Fink, J.H., 1985. Geometry of silicic dikes beneath the Inyo Domes, California. Journal of Geophysical Research 90, 11,127–11,133.

Fossen, H., 2010. Deformation bands formed during soft-sediment deformation: observations from SE Utah. Marine and Petroleum Geology 27, 215–222.
Fossen, H., Hesthammer, J., 1997. Geometric analysis and scaling relations of deformation bands in porous sandstone. Journal of Structural Geology 19, 1479–1493.
Fossen, H., Schultz, R.A., Shipton, Z.K., Mair, K., 2007. Deformation bands in sandstone: a review. Journal of the Geological Society, London 164, 755–769.
Fossen, H., Schultz, R.A., Torabi, A., 2011. Conditions and implications for compaction band formation in Navajo Sandstone, Utah. Journal of Structural Geology 33, 1477–1490.
Gudmundsson, A., 2004. Effects of Young's modulus on fault displacement. Comptes Rendus de Geoscience 336, 85–92.
Hatton, C.G., Main, I.G., Meredith, P.G., 1994. Non-universal scaling of fracture length and opening displacement. Nature 367, 160–162.
Ikari, M.J., Marone, C., Saffer, D.M., 2011. On the relation between fault strength and frictional stability. Geology 39, 83–86.
Jamison, W.R., 1989. Fault-fracture strain in Wingate Sandstone. Journal of Structural Geology 11, 959–974.
Japsen, P., Dysthe, D.K., Hartz, E.H., Stipp, S.L.S., Yarushina, V.M., Jamtveit, B., 2011. A compaction front in North Sea chalk. Journal of Geophysical Research 116, B11208. http://dx.doi.org/10.1029/2011JB008564.
Kachanov, M., 1992. Effective elastic properties of cracked solids: critical review of some basic concepts. Applied Mechanics Reviews 45, 304–335.
Kaproth, B.M., Cashman, S.M., Marone, C., 2010. Deformation band formation and strength evolution in unlithified sand: the role of grain breakage. Journal of Geophysical Research 115, B12103. http://dx.doi.org/10.1029/2010JB007406.
Kim, Y.-S., Sanderson, D.J., 2005. The relationship between displacement and length of faults: a review. Earth-Science Reviews 68, 317–334.
Kim, Y.-S., Peacock, D.C.P., Sanderson, D.J., 2004. Fault damage zones. Journal of Structural Geology 26, 503–517.
Klimczak, C., Schultz, R.A., Parashar, R., Reeves, D.M., 2010. Cubic law with aperture-length correlation: implications for network scale fluid flow. Hydrogeology Journal 18, 851–862. http://dx.doi.org/10.1007/s10040–009–0572–6.
Kohlstedt, D.L., Evans, B., Mackwell, S.J., 1995. Strength of the lithosphere: constraints imposed by laboratory experiments. Journal of Geophysical Research 100, 17,587–17,602.
Krantz, R.W., 1988. Multiple fault sets and three-dimensional strain: theory and application. Journal of Structural Geology 10, 225–237.
Krantz, R.W., 1989. Orthorhombic fault patterns: the odd axis model and slip vector orientations. Tectonics 8, 483–495.
Leblond, J.-B., Karma, A., Lazarus, V., 2011. Theoretical analysis of crack front instability in mode I+III. Journal of the Mechanics and Physics of Solids 59, 1872–1887.
Long, J.J., Imber, J., 2011. Geological controls on fault relay zone scaling. Journal of Structural Geology 33, 1790–1800.
Mazars, J., Pijaudier-Cabot, G., 1996. From damage to fracture mechanics and conversely: a combined approach. International Journal of Solids and Structures 33, 3327–3342.
McEwen, A.S., Eliason, E.M., Bergstrom, J.W., Bridges, N.T., Hansen, C.J., Delamere, W.A., Grant, J.A., Gulick, V.C., Herkenhoff, K.E., Keszthelyi, L., Kirk, R.L., Mellon, M.T., Squyres, S.W., Thomas, N., Weitz, C.M., 2007. Mars Reconnaissance Orbiter's High Resolution Imaging Science Experiment (HiRISE). Journal of Geophysical Research 112, E05S02. http://dx.doi.org/10.1029/2005JE002605.
Moros, J.G., 1999. Relationship between fracture aperture and length in sedimentary rocks. Unpublished M.S. thesis., The University of Texas, Austin.
Navidi, W., 2006. Statistics for Engineers and Scientists. McGraw Hill, New York.
Nicholson, R., Pollard, D.D., 1985. Dilation and linkage of echelon cracks. Journal of Structural Geology 7, 583–590.
Nicol, A., Watterson, J., Walsh, J.J., Childs, C., 1996. The shapes, major axis orientations and displacement patterns of fault surfaces. Journal of Structural Geology 18, 235–248.
Nicol, A., Walsh, J.J., Villamor, P., Seebeck, H., Berryman, K.R., 2010. Normal fault interactions, paleoearthquakes and growth in an active rift. Journal of Structural Geology 21, 1101–1113.
Okubo, C.H., 2010. Structural analysis of Amazonian-aged layered deposits in southwest Candor Chasma. Icarus 207, 210–255.
Okubo, C.H., Martel, S.J., 1998. Pit crater formation on Kilauea volcano, Hawaii. Journal of Volcanology and Geothermal Research 86, 1–18.
Okubo, C.H., Schultz, R.A., 2005. Evolution of damage zone geometry and intensity in porous sandstone: insight from strain energy density. Journal of the Geological Society, London 162, 939–949.
Olson, J.E., 2003. Sublinear scaling of fracture aperture versus length: an exception or the rule? Journal of Geophysical Research 108, 2413. http://dx.doi.org/10.1029/2001JB000419.
Olson, J.E., Schultz, R.A., 2011. Comment on "A note on the scaling relations for opening mode fractures in rock" by C.H. Scholz. Journal of Structural Geology 33, 1523–1524.
Petit, J.-P., Laville, E., 1987. Morphology and microstructures of hydroplastic slickensides in sandstone. In: Jones, M.E., Preston, R.M.F. (Eds.), Deformation of Sediments and Sedimentary Rocks. Geological Society Special Publication, vol. 29, pp. 107–121.
Petit, J.-P., Massonat, G., Pueo, F., Rawnsley, K., 1994. Rapport de forme des fractures en mode I dans les roches stratifiées: une étude de cas dans le bassin permien de Lodève (France). Bulletin Elf Aquitaine Production 18, 211–229.
Pollard, D.D., 1987. Elementary fracture mechanics applied to the structural interpretation of dykes. In: Halls, H.C., Fahrig, W.F. (Eds.), Mafic Dyke Swarms, Geological Association of Canada, Special Paper 34, pp. 5–24.
Pollard, D.D., Bergbauer, S., Mynatt, I., 2004. Using differential geometry to characterize and analyse the morphology of joints. In: Cosgrove, J.W., Engelder, T. (Eds.), The Initiation, Propagation, and Arrest of Joints and Other Fractures. Geological Society, London, Special Publications, vol. 231, pp. 153–182.
Renshaw, C.E., Park, J.C., 1997. Effect of mechanical interactions on the scaling of fracture length and aperture. Nature 386, 482–484.
Rotevatn, A., Fossen, H., 2012. Soft faults with hard tips: magnitude-order displacement gradient variations controlled by strain softening versus hardening; implications for fault scaling. Journal of the Geological Society, London 169, 123–126.
Rubin, A.M., 1993. Tensile fracture of rock at high confining pressure: implications for dike propagation. Journal of Geophysical Research 98, 15,919–15,925.
Rubin, A.M., 1995. Propagation of magma-filled cracks. Annual Review of Earth and Planetary Sciences 23, 287–336.
Rudnicki, J.W., 2007. Models for compaction band propagation. In: David, C., Le Ravalec-Dupin, M. (Eds.), Rock Physics and Geomechanics in the Study of Reservoirs and Repositories. Geological Society of London Special Publication, vol. 284, pp. 107–125.
Rudnicki, J.W., Sternlof, K.R., 2005. Energy release model of compaction band propagation. Geophysical Research Letters 32, L16303. http://dx.doi.org/10.1029/2005GL023602.
Rudnicki, J.W., Tembe, S., Wong, T.-f., 2006. Relation between width and length of compaction bands in porous sandstones (abstract). Eos (Transactions AGU) 87, T43A–T1633.
Scholz, C.H., 2002. The Mechanics of Earthquakes and Faulting, second ed. Cambridge University Press, 471 pp.
Scholz, C.H., 2010. A note on the scaling relations for opening mode fractures in rock. Journal of Structural Geology 32, 1485–1487.
Scholz, C.H., 2011. Reply to comments of Jon Olson and Richard Schultz. Journal of Structural Geology 33, 1525–1526.
Schultz, R.A., 1999. Understanding the process of faulting: selected challenges and opportunities at the edge of the 21st century. Journal of Structural Geology 21, 985–993.
Schultz, R.A., 2009. Scaling and paleodepth of compaction bands, Nevada and Utah. Journal of Geophysical Research 114, B03407. http://dx.doi.org/10.1029/2008JB005876.
Schultz, R.A., Fossen, H., 2002. Displacement-length scaling in three dimensions: the importance of aspect ratio and application to deformation bands. Journal of Structural Geology 24, 1389–1411.
Schultz, R.A., Fossen, H., 2008. Terminology for structural discontinuities. American Association of Petroleum Geologists Bulletin 92, 853–867.
Schultz, R.A., Soliva, R., 2012. Propagation energies inferred from deformation bands in sandstone. International Journal of Fracture 176, 135–149.
Schultz, R.A., Okubo, C.H., Wilkins, S.J., 2006. Displacement-length scaling relations for faults on the terrestrial planets. Journal of Structural Geology 28, 2182–2193.
Schultz, R.A., Soliva, R., Fossen, H., Okubo, C.H., Reeves, D.M., 2008a. Dependence of displacement-length scaling relations for fractures and deformation bands on the volumetric changes across them. Journal of Structural Geology 30, 1405–1411.
Schultz, R.A., Mège, D., Diot, H., 2008b. Emplacement conditions of igneous dikes in Ethiopian Traps. Journal of Volcanology and Geothermal Research 178, 673–692.
Schultz, R.A., Hauber, E., Kattenhorn, S., Okubo, C.H., Watters, T.R., 2010. Interpretation and analysis of planetary structures. Journal of Structural Geology 32, 855–875.
Soliva, R., Benedicto, A., 2004. A linkage criterion for segmented normal faults. Journal of Structural Geology 26, 2251–2267.
Soliva, R., Schultz, R.A., 2008. Distributed and localized faulting in extensional settings: insight from the North Ethiopian Rift – Afar transition area. Tectonics 27, TC2003. http://dx.doi.org/10.1029/2007TC002148.
Soliva, R., Schultz, R.A., Benedicto, A., 2005. Three-dimensional displacement-length scaling and maximum dimension of normal faults in layered rocks. Geophysical Research Letters 32, L16302. http://dx.doi.org/10.1029/2005GL023007.
Soliva, R., Schultz, R.A., Ballas, G., Taboada, A., Wibberley, C., Saillet, E., Benedicto, A. A model of strain localization in porous sandstone as a function of tectonic setting, burial and material properties; new insight from Provence (southern France). Journal of Structural Geology., in press.
Sternlof, K.R., Rudnicki, J.W., Pollard, D.D., 2005. Anticrack inclusion model for compaction bands in sandstone. Journal of Geophysical Research 110, B11403. http://dx.doi.org/10.1029/2005JB003764.
Tembe, S., Baud, P., Wong, T.-f, 2008. Stress conditions for the propagation of discrete compaction bands in porous sandstone. Journal of Geophysical Research 113, B09409. http://dx.doi.org/10.1029/2007JB005439.
Tondi, E., Antonellini, M., Aydin, A., Marchegiani, L., Cello, G., 2006. The role of deformation bands, stylolites and sheared stylolites in fault development in carbonate grainstones of Majella Mountain, Italy. Journal of Structural Geology 28, 376–391.
Tondi, E., Cilona, A., Agosta, F., Aydin, A., Rustichelli, A., Renda, P., Giunta, G., 2012. Growth processes, dimensional parameters and scaling relationships of two

conjugate sets of compactive shear bands in porous carbonate grainstones, Favignana Island, Italy. Journal of Structural Geology 37, 53–64.
Twiss, R.J., Marrett, R., 2010. Determining brittle extension and shear strain using fault length and displacement systematics: part II: data evaluation and test of the theory. Journal of Structural Geology 32, 1978–1995.
Vermilye, J.M., Scholz, C.H., 1995. Relation between vein length and aperture. Journal of Structural Geology 17, 423–434.
Weinberger, R., Lyakhovsky, V., Baer, G., Agnon, A., 2000. Damage zones around en echelon dike segments in porous sandstone. Journal of Geophysical Research 105, 3115–3133.
Welch, M.J., Davies, R.K., Knipe, R.J., Tueckmantel, C., 2009. A dynamic model for fault nucleation and propagation in a mechanically layered section. Tectonophysics 474, 473–492.
Wesnousky, S.G., 1988. Seismological and structural evolution of strike-slip faults. Nature 335, 340–343.
Wibberley, C.A.J., Petit, J.-P., Rives, T., 1999. Mechanics of high displacement gradient faulting prior to lithification. Journal of Structural Geology 21, 251–257.
Wibberley, C.A.J., Petit, J.-P., Rives, T., 2000. Mechanics of cataclastic 'deformation band' faulting in high-porosity sandstone, Provence. Earth and Planetary Sciences 331, 419–425.
Willemse, E.J.M., 1997. Segmented normal faults: correspondence between three-dimensional mechanical models and field data. Journal of Geophysical Research 102, 675–692.
Willemse, E.J.M., Pollard, D.D., Aydin, A., 1996. Three-dimensional analyses of slip distributions on normal fault arrays with consequences for fault scaling. Journal of Structural Geology 18, 295–309.
Wong, T.-f., Baud, P., 2012. The brittle-ductile transition in porous rock: a review. Journal of Structural Geology 44, 25–53.
Xu, S.-S., Nieto-Samaniego, A.F., Alaniz-Álvarez, S.A., Velasquillo-Martínez, L.G., 2005. Effect of sampling and linkage on fault length and length-displacement relationship. International Journal of Earth Sciences 95, 841–853.
Zoback, M.D., 2007. Reservoir Geomechanics. Cambridge University Press. 449 p.
Zhao, X.G., Cai, M., 2010. A mobilized dilation angle model for rocks. International Journal of Rock Mechanics & Mining Sciences 47, 368–384.